RSC Advances

ROYAL SOCIETY OF CHEMISTRY

www.rsc.org/advances

Journal Name

ARTICLE

Photocatalysis of $NaYF_4$: Yb,Er/CdSe Composites under 1560 nm Laser Excitation

Received 00th January 20xx,
Accepted 00th January 20xx

DOI: 10.1039/x0xx00000x

www.rsc.org/

Xingyuan Guo,[a,b,d] Changfeng Chen,[d] Daqi Zhang,[c] Carl P. Tripp,[d] Shengyan Yin,[a] Weiping Qin*[a]

The most common materials used to generate near-infrared-driven photocatalysis occur by 980 nm laser excitation of composites that are a combination of a semiconductor with upconverting luminescence particles. The challenge remains to increase the light harvest efficiency, and thus, it is necessary to extend the absorption spectra of photocatalysts. In this work, $NaYF_4$: Yb,Er/CdSe composites were prepared by depositing CdSe nanocrystals onto the surface of $NaYF_4$:Yb,Er microcrystals. UV and Visible emission of light resulted from multiphoton upconverting processes in Er^{3+} under 1560 nm laser irradiation, which, in turn, activated the CdSe catalyst. The energy transfer between $NaYF_4$: Yb,Er and CdSe was investigated by steady-state and dynamic fluorescence spectroscopy. The photocatalytic performance was investigated by the degradation of methylene blue in aqueous solution. These results show that Er coupled with semiconductor heterojunctions provides a photocatalyst that operates in the extended near-infrared range.

1. Introduction

Near-infrared (NIR) photocatalysts, using direct NIR-to-Visible radiation or generating UV radiation through upconversion to provide the necessary energy to a semiconductor, are a new research area in the field of photocatalysis and photoelectrochemical water splitting.[1-5] The application of an upconversion process using phosphor-like systems would lead to an increase in the photocatalytic performance of traditional UV or visible active photocatalysts. This occurs because the light absorption range is effectively extended to the infrared range, which accounts for nearly half of the solar energy output. In our previous work, we reported the NIR-driven photocatalysis of broadband and heterojunction composites of semiconductors combined with upconverting luminescence particles.[6-9] Using this strategy, the direct absorption of NIR light by the semiconductor (E_g > 2.0 eV) does not occur, but when combined with upconverting materials, the same semiconductors showed photocatalytic properties under illumination of NIR light sources. From our initial work,[6] other materials such as $NaYF_4$:Yb,Tm/CdS,[10] Er:$YAlO_3$/ZnO,[11] Er-doped $BiVO_4$,[12] CaF_2: Yb, Er/TiO_2[13] and $NaYF_4$:Yb,Tm@TiO_2,[14] have been generated and shown to operate with NIR irradiation. However, all these studies have used 980 nm laser excitation. Therefore, from the viewpoint of harvesting solar energies, it is desirable to extend the light absorption spectra of photocatalysts to operate over a broader range of the NIR solar spectrum.

The main hurdle limiting widespread usage of these materials is their low photocatalytic efficiency under NIR illumination. This means that the contribution of the upconverted photons to the overall efficiency compared to UV and visible photocatalysts would be small, on the order of 1-3%. However, NIR upconversion materials have potential application in the diagnosis and photodynamic therapy of cancers[15-18] because of the much higher penetration depth of NIR into tissue compared to both UV and visible radiation. For example, inorganic upconversion nanoparticles have been extensively used for *in vivo* detection and visualization of diverse animal cells and bio-tissues. This field has been expanding rapidly and is discussed in several excellent reviews published in recent years.[19, 20] In particular, Xu *et al*. reported that 1600-1800 nm radiation have additional advantages for *in vivo* measurements.[21] In this spectral window, light scattering by the tissue is small relative to both UV and Visible light, which increases the penetration depth as well as improves the focusing capability of the NIR light. As a result, development of materials in exhibit upconversion at 1560 nm could be disable in the imaging or therapy of brain cell and blood vessels residing in a > 150 μm thick brain tissue section.[22]

In this paper, NIR photocatalysts of $NaYF_4$: Yb,Er/CdSe composites were synthesized using a two-step hydrothermal method. CdSe nanocrystals were linked onto the surfaces of the $NaYF_4$: Yb,Er microcrystals. The energy transfer between $NaYF_4$: Yb,Er and CdSe was investigated by steady-state and dynamic fluorescence spectroscopy. The photocatalytic activities of the composites were evaluated by the degradation of methylene blue aqueous solutions under 1560 nm NIR irradiation. Designing materials such as those reported here that can operate over a wider range of NIR wavelengths will help in the design of photovoltaic devices that cover a broader region of the solar spectrum.

2. Experimental

2.1 Materials

[a]*State Key Laboratory on Integrated Optoelectronics, College of Electronic Science and Engineering, Jilin University, Changchun, 130012, China*
[b]*College of Physics, Jilin University, Changchun, 130012, China*
[c]*Department Of Thyroid Surgery, china-Japan Union Hospital Of Jilin University; Jilin Provincial Key Laboratory Of Surgical Translational Medicine. Changchun, 130033, China*
[d]*Laboratory for Surface Science and Technology and Department of Chemistry, University of Maine, Orono ME 04468, USA*
wpqin@jlu.edu.cn (W. Qin) Tel: 86-431-85168240-8325, Fax: 86-431-85168240-8325

Yttrium oxide (Y_2O_3), ytterbium oxides (Yb_2O_3) and erbium oxide (Er_2O_3) were obtained from the Shandong Yutai Fine Chemical Factory at 99.999% purity. Sodium fluoride (NaF) and ethylenediamine tetraacetic acid (EDTA) were obtained from the Beijing Chemical Reagent Factory. Cadmium chloride ($CdCl_2$), selenium powder, sodium borohydride ($NaBH_4$) and thiolglycolic acid (TGA) were purchased from the Tianjin Guangfu Fine Chemical Research Institute and used without further purification.

2.2 Synthesis of $NaYF_4$: Yb,Er microcrystals

$NaYF_4$:Yb,Er microcrystals were synthesized *via* the ethylene tetraacetic acid (EDTA) assisted hydrothermal method, described elsewhere.[23] Briefly, 10 mL of 0.5 mmol $Y(NO_3)_3$, $Yb(NO_3)_3$ and $Er(NO_3)_3$ (Y:Yb:Er = 79:20:1) were added to 20 mL of 0.25 mmol EDTA in deionized water. The solution was stirred for 1 h to allow for the formation of a chelated RE–EDTA complex. Next, 20 mL of 0.5 M NaF solution was added to the solution to generate a RE^{3+}:F^- ratio of 1:16. After stirring for 0.5 h, the mixture was transferred to a 50 mL Teflon-lined stainless steel autoclave. The autoclave was sealed and placed in an oven at 160 °C for 18 h, and then cooled to room temperature in air. The white colored product was centrifuged and washed with deionized water and ethanol three times, followed by drying in air drying at 60 °C for 20 h. Finally, the sample was annealed at 400 °C for 1.5 h under an argon atmosphere.

2.3 Synthesis of CdSe nanocrystals

The preparation procedures of the CdSe nanocrystals are described elsewhere.[24] Briefly, 0.47 g $CdCl_2 \cdot 5H_2O$ was dissolved in 100 mL deionized water, in a 250 mL three-neck flask under stirring and 0.5 mL TGA was then added dropwise. The pH of the solution was adjusted to 10.3, using 1.0 mol·L^{-1} NaOH. Next, the solution was bubbled with N_2 for 30 min. Then, 1.0 mL of 1M oxygen-free NaHSe was injected, using a syringe into the vigorously stirred solution. The turning of the solution color from white to orange indicated the production of CdSe nanocrystals. The product was centrifuged at 8500 rpm and washed with deionized water and ethanol 3 times. The product was finally dried under vacuum at 60 °C for 10 h.

2.4 The preparation of $NaYF_4$: Yb,Er/CdSe composite

$NaYF_4$: Yb,Er/CdSe composites were fabricated using a method described elsewhere.[10] Typically, 500 mg of $NaYF_4$: Yb,Er microcrystals were dispersed in 20 mL deionized water containing 0.2 mL mercaptoethanol. After stirring for 3 h, the product was separated and washed. In a separate beaker, 100 mg of CdSe nanoparticles were dispersed in 10 mL deionized water containing 0.1mL thioglycolic acid. The solution was stirred for 3 h, and then centrifuged and washed.

The $NaYF_4$: Yb,Er microcrystals and CdSe nanoparticles were mixed in 20 mL deionized water, and heated at 160 °C for 3 h. The products were collected by centrifugation and washed with deionized water several times.

2.5 Characterizations

The crystal structures of the $NaYF_4$: Yb,Er/CdSe composite were analyzed by a Rigaku RU-200b X-ray powder diffraction (XRD), using a nickel-filtered Cu Kα radiation (λ = 1.5418 Å). The size and morphology were characterized by SEM (JEOL-7500F with operating voltage of 15 kV) and TEM (JEM2000-EX, 100kV). Energy dispersive X-ray （EDX）scan profiles were obtained on a JSM-7500F microscope coupled with an EDX spectrometer (Genesis Apollo XL). The absorption spectra were recorded with a UV-vis spectrophotometer (Shimadzu UV-3600). The emission spectra were recorded with a spectrophotometer (Hitachi F-4500) equipped with a Hamamatsu R928 photomultiplier and a 1560 nm continuous wave diode laser. The luminescence decays was studied by using a 1579 nm Raman shifter laser (pumped by the second harmonic of a Nd:YAG pulsed laser, pulse width 10 ns, repetition rate 10 Hz). All above measurements were performed at room temperature.

2.6 The evaluation of the photocatalytical activity

The photocatalytical activity of the $NaYF_4$: Yb,Er/CdSe composite material was evaluated using the degradation of methylene blue (MB) in aqueous solution. In a typical experiment, 0.5 mg of $NaYF_4$:Yb,Er/CdSe composite particles was dispersed into a quartz vial containing 0.5 mL 15 mg L^{-1} MB aqueous solution. Prior to irradiation, the vial was kept in the dark for 12 h for establishing adsorption-desorption equilibrium of MB on the surface of the photocatalysts. A diode laser at 1560 nm, with a power density of 2.0 W/cm^2, was used as the NIR source. After each 5 h irradiation, 0.3 mL aliquot of MB aqueous solution was extracted for UV-vis absorbance measurement. The sample was returned to the quartz vial after recording the UV spectrum. The dye concentration was measured with a UV-Vis spectrometer, using the absorption peak at 665 nm. For comparison, the NIR-responsive photo degradation of MB, using CdSe and $NaYF_4$: Yb,Er, were also measured by the same procedures above, respectively.

3. Results and discussion

3.1 Structure characterizations

The crystal structure of CdSe nanocrystals, and $NaYF_4$: Yb,Er/CdSe composites were determined by XRD. As shown in Fig. 1(a), the XRD patterns of the CdSe nanoparticles were in a good agreement with the hexagonal phase CdSe (JCPDS No. 77-2307). Fig. 1(b) shows an XRD pattern of the $NaYF_4$: Yb,Er/CdSe composite. The pattern is dominated by peaks associated with the hexagonal phase of $NaYF_4$ (JCPDS No. 28-1192), while weak diffraction peaks of CdSe are observed at 25º.

The morphologies of $NaYF_4$: Yb,Er microcrystals and $NaYF_4$:Yb,Er/CdSe composites were characterized by SEM and TEM. Fig. 2(a) shows that the $NaYF_4$: Yb,Er microcrystals are hexagonal pillars with a uniform dimension of ~2 μm in length and ~1 μm in diameter. Fig. 2(b) show the SEM images of the $NaYF_4$: Yb,Er/CdSe composites. EDX was employed to further analyze the elemental composition of the $NaYF_4$: Yb,Er/CdSe composites (Fig. 2(c)), which suggests that the composites consist of Yb, Er, Na, Y, F, Cd and Se elements. Fig 2(d) and 2(e) are the TEM images of $NaYF_4$:Yb,Er/CdSe composites at various magnifications The TEM image in Fig. 2(e) shows that on the surface of the $NaYF_4$: Yb,Er/CdSe composites is a 50-nm-thickness layer of tightly interconnected nanoparticles with a size of 6~8 nm. Moreover, high-resolution transmission electron micrographs (HR-TEM) (Fig. 2(f)) show that these nanoparticles are composed of CdSe NPs. In particular, a lattice of 0.35 nm corresponded to the interplanar distance of the (001) lattice plane of the hexagonal CdSe phase.

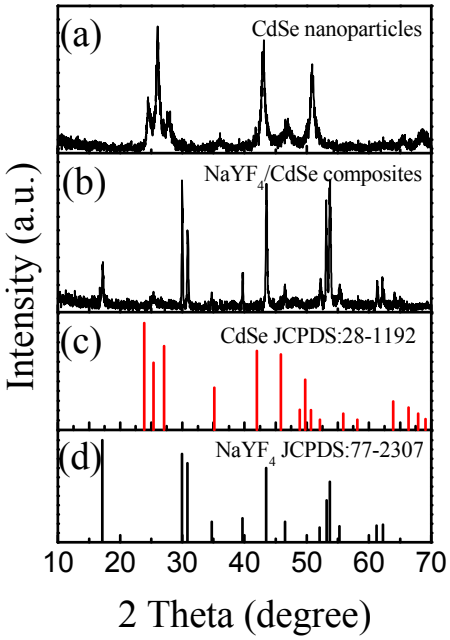

Fig. 1 The XRD patterns of (a) the CdSe nanoparticles, (b) the $NaYF_4$: Yb,Er/CdSe composites, (c) JCPDS no.28-1192, (d) JCPDS no.77-2307.

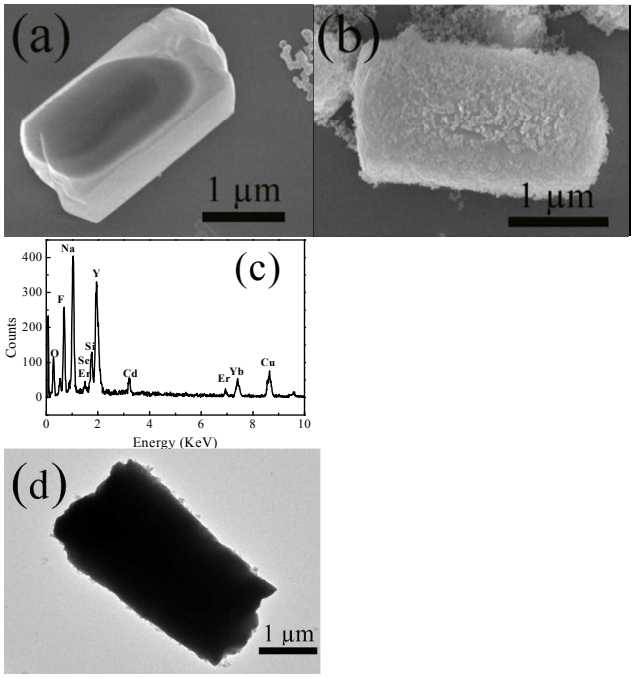

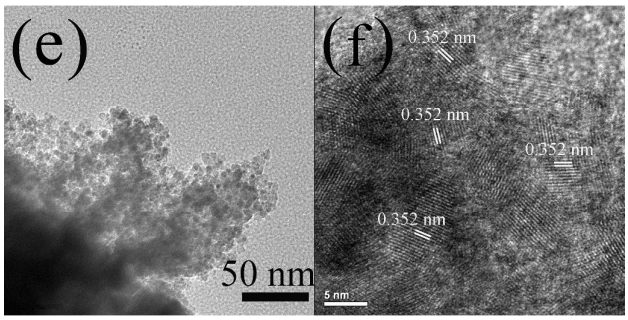

Fig. 2 SEM images of (a) $NaYF_4$: Yb,Er microcrystals and (b) $NaYF_4$:Yb,Er/CdSe composites; (c), EDX pattern of sample shown in (d) and (e) which are the TEM images of $NaYF_4$:Yb,Er/CdSe composites at various magnifications; (f) HRTEM image of CdSe nanocrystals on the $NaYF_4$:Yb,Er surface.

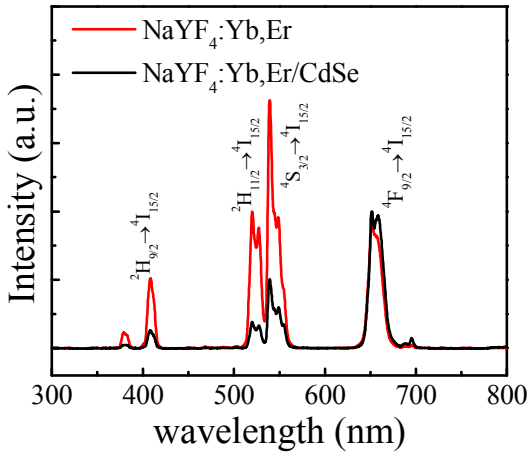

Fig. 3 Photoluminescence spectra of $NaYF_4$: Yb,Er microcrystals (black) and $NaYF_4$:Yb,Er/CdSe composites (red) under 1560 nm excitation at room temperature.

3.2 Photoluminescence properties

Fig. 3 shows the upconverted emission spectra of $NaYF_4$: Yb,Er microcrystals and $NaYF_4$:Yb,Er/CdSe composites under 1560 nm excitation. In the spectrum of $NaYF_4$: Yb,Er microcrystals, five emission peaks located at 379 nm (3.272 eV), 408 nm (3.039 eV), 520 nm (2.385 eV), 539 nm (2.301 eV) and 664 nm (1.867 eV) correspond to $^4G_{11/2} \rightarrow {}^4I_{15/2}$, $^2H_{9/2} \rightarrow {}^4I_{15/2}$, $^2H_{11/2} \rightarrow {}^4I_{15/2}$, $^4S_{3/2} \rightarrow {}^4I_{15/2}$ and $^4F_{9/2} \rightarrow {}^4I_{15/2}$ transitions of Er^{3+} ions, respectively.[25] For comparison, the two spectra in Fig.3 were normalized using the red emission of Er^{3+} ions at 664 nm (1.867 eV), as the excited state energy of 664 nm is lower than that of the CdSe nanocrystals acceptor and thus, should not be absorbed by CdSe nanocrystals.[26, 27] It was found that the emission spectrum of $NaYF_4$: Yb,Er/CdSe composites is different from that of $NaYF_4$:Yb,Er microcrystals. The intensities of the emission peaks at 379 nm, 408 nm, 520 nm and 539 nm for $NaYF_4$: Yb,Er decrease after the incorporation of CdSe nanocrystals, compared to the red emission of Er^{3+} at 660 nm which did not change, as the energy of this excited state is lower than that of the CdSe acceptor.[27] Specifically, for $NaYF_4$: Yb,Er, the decrease in fluorescence intensity ratio were calculated using the equation, $I_{decay}=1 - I_{coated}/I_{uncoated,}$. Where $I_{uncoated}$ and I_{coated} are the intensity of the emission peak in $NaYF_4$: Yb,Er without and with CdSe,

respectively.The intensity decay values of I_{decay} for the 408, 520 and 539 nm peaks are calculated to be 0.75, 0.80 and 0.45, respectively. This decrease in fluorescence shows the presence of an energy transfer from $NaYF_4$: Yb,Er to CdSe.

3.3 UV-Vis spectra

UV-vis absorption spectra of $NaYF_4$: Yb,Er/CdSe composites and CdSe nanoparticles are shown in Fig. 4. The band-gap absorption peaks at ~ 620 nm (2.0 eV) are characteristic of the CdSe nanoparticles.[28] the peak at 976nm is associated with $^2F_{5/2} \rightarrow {}^2F_{7/2}$ transition of Yb^{3+}.[29] As the energies of the excited states of Er^{3+} ions at $^4G_{11/2}$ (3.272 eV), $^2H_{9/2}$ (2.981 eV), $^2H_{11/2}$ (2.322 eV) and $^4S_{3/2}$ (2.246 eV) are larger than that of the CdSe bandgap, the excited energy of Er^{3+} exceeds with the bandgap of CdSe, and thus, can be absorbed by CdSe via energy transfer.

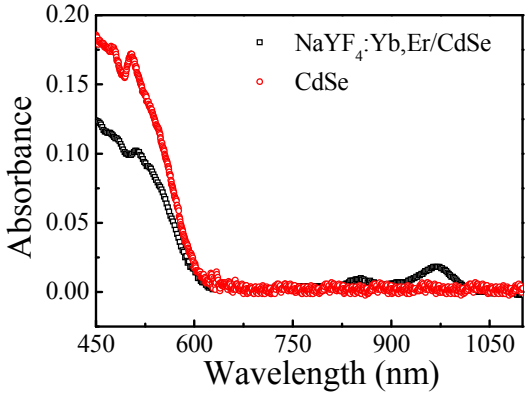

Fig. 4 UV-Vis spectrum of CdSe and $NaYF_4$: Yb,Er/CdSe composites.

3.4 Energy transfer

To demonstrate the energy transfer process between $NaYF_4$: Yb,Er and CdSe, the time-resolved fluorescence decay of the $^2H_{9/2}$, $^2H_{11/2}$, $^4S_{3/2}$ and $^4F_{9/2}$ levels of Er^{3+} was measured and shown in Fig 5. Accelerated decay rates were found for the $^2H_{9/2}$, $^2H_{11/2}$, $^4S_{3/2}$ excited states in $NaYF_4$: Yb,Er/CdSe composite (see Fig 5 (a,b,c)), while identical decay rates were found for the $^4F_{9/2}$ of Er^{3+} between $NaYF_4$: Yb,Er/CdSe composite and pure $NaYF_4$: Yb,Er (see Fig. 5d). This is consistent with the results from the emission spectra (Fig. 3). that a significant decrease in the emission intensity of $^2H_{9/2}$, $^2H_{11/2}$, $^4S_{3/2}$ was found in $NaYF_4$: Yb,Er/CdSe composites after the incorporation of CdSe. These results also suggest the presence of the Förster resonance energy transfer (FRET) between $NaYF_4$: Yb,Er and CdSe.[26] The efficiency of energy transfer was calculated using the equation $E_{decay}=1-\tau_{coated}/\tau_{uncoated}$, where τ_{coated} and $\tau_{uncoated}$ are the lifetime of the excited states in $NaYF_4$: Yb,Er with and without CdSe, respectively.[30] The lifetime of excited state of luminescence centers, τ, depends on the radiative transition rate (W_R), the nonradiative transition rate (W_{NR}) and the energy transfer rate, which can be expressed as $\tau=1/(W_R + W_{NR} + W_{ET})$.[31, 32] As shown in Table 1, the calculated energy transfer efficiencies for $^2H_{9/2}$, $^2H_{15/2}$, $^4S_{3/2}$ and $^4F_{9/2}$ levels were 0.36, 0.35, 0.20, and 0, respectively,. These values are much lower than the I_{decay}, which were calculated to be 0.75, 0.80 and 0.45. This suggests that two mechanisms of energy transfer from the Er^{3+} ions to CdSe are present. One process is FRET. In this case, the presence of CdSe in contact with the $NaYF_4$: Yb,Er microcrystals creates a nonradiative energy transfer channel from the excited state of Er^{3+} to CdSe. Such an energy transfer process lead to the acceleration of the relaxation of the excited state of Er^{3+}, leading to an increase in the overall transition rate and thus, the reduction of fluorescence lifetime. This provides evidence that FRET takes place.[26] The other process corresponds to a photon reabsorption (PR) process, where the emitted photons from Er^{3+} are adsorbed by the semiconductors.

3.5 Photocatalytic activity

MB was used as a model pollutant to investigate the photocatalytic activity of $NaYF_4$: Yb,Er/CdSe under NIR irradiation of 1560 nm. Fig. 6(a) shows the absorbance spectra of MB catalysed by the $NaYF_4$: Yb,Er/CdSe composites as a function of irradiation time

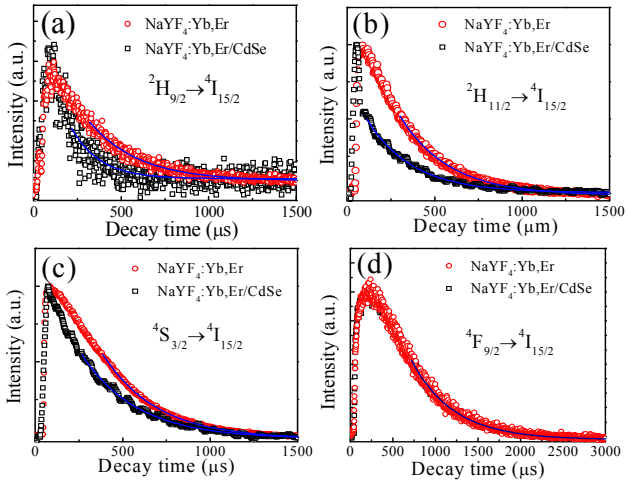

Fig. 5 Luminescence dynamic curves form the $^2H_{9/2}$ (a), $^2H_{11/2}$ (b), $^4S_{3/2}$ (c) and $^4F_{9/2}$ (d) of Er^{3+} ions in $NaYF_4$:Yb,Er microcrystals and $NaYF_4$:Yb,Er/CdSe composites under the excitation of a 1579 nm pulsed Raman shift laser.

under 1560 nm irradiation. The intensity of the band at 650 nm, due to MB, decreased with an increase in the NIR irradiation time. A 65% degradation of MB was found for $NaYF_4$: Yb,Er/CdSe composites after 30 h irradiation.

The degradation efficiency can be evaluated through the time dependent change of the concentration of MB during the NIR irradiation relative to the original MB. Fig. 6(b) shows the time dependent value of C/C_0, where C_0 is the original concentration of MB and C is the concentration of MB irradiated with a 1560 nm laser for time (t).

It is well known that NIR irradiation and nonradiative relaxation of excited Yb^{3+} and Er^{3+} ions can generate thermal energy. To verify whether the thermal energy dominated the degradation of MB, control experiments of MB in the presence of $NaYF_4$: Yb,Er with NIR radiation were performed. As shown in Fig. 6(b), these solutions showed very limited activities (2%) in the degradation of MB after 30 h irradiation.

This suggests that the thermal energy generated by a 1560 nm laser irradiation is not sufficient to induce the thermal degradation of MB. As a result, the degradation of MB by upconverting/semiconductor composite catalysts induced

predominately by photocatalysis rather than photolysis or thermolysis. The degradation of MB under 980 nm radiation was also performed. There was showed 75% activity in the degradation of MB after 30 h irradiation.

Table 1 Lifetimes of $^2H_{9/2}$, $^2H_{11/2}$, $^4S_{3/2}$ and $^4F_{9/2}$ levels of Er^{3+} in $NaYF_4$: Yb^{3+},Er^{3+} microcrystals and $NaYF_4$: Yb^{3+}, Er^{3+}/CdSe composites from variations in Fig.5.

Lifetime (μs) / Samples	Energy level			
	$^2H_{9/2}$	$^2H_{15/2}$	$^4S_{3/2}$	$^4F_{9/2}$
$NaYF_4$:Yb,Er	324	304	405	495
$NaYF_4$:Yb,Er/CdSe	210	196	323	495
E_{decay}	0.36	0.3	0.20	0
I_{decay}	0.75	0.8	0.45	0

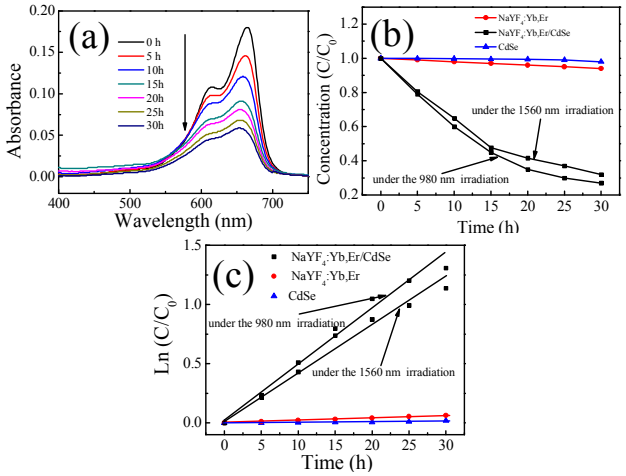

Fig. 6 (a) Absorbance spectra of MB catalyzed by $NaYF_4$:Yb,Er/CdSe composites as a function of the irradiation time under 1560 nm laser; (b) Normalized concentration of MB decomposed by CdSe, $NaYF_4$:Yb,Er and $NaYF_4$:Yb,Er/CdSe (1560 nm and 980 nm irradiation). (c) The kinetic data for the photodegradation of MB.

The reaction kinetics for the MB photodegradation were fitted using a Langmuir-Hinshelwood kinetic model. The rate constants were calculated to be 3.5×10^{-4} (min^{-1}) and 8.0×10^{-4} (min^{-1}) for $NaYF_4$: Yb,Er/CdSe under the 1560 nm and 980 nm laser irradiation, respectively. Compared to our previous research result,[9] the rate constants of $NaYF_4$: Yb,Tm/CdS were calculated to be 3.38×10^{-4} (min^{-1}) under the 980 nm laser irradiation.

There are two factors that can used to explain the reason for the rate constants. First, the population of the states $^1I_6$, $^1D_2$, and $^1G_4$ of Tm^{3+} are due to five-photon, four-photon, and three-photon UC processes under 980 nm laser irradiation, respectively.[33] In contrast, the population of the states $^2H_{9/2}$, $^2H_{15/2}$ and $^4S_{3/2}$ of Er^{3+} are all due to four-photon, UC processes under 1560 nm laser irradiation.[34] However, two photons are needed to excite Yb^{3+} ions to the $^2F_{5/2}$ state from their ground state $^2F_{7/2}$ under 1560 nm excitation, while only one photon is required under 980 nm excitation. As a result, the UV or Visible UC emissions under 1560 excitation are of lower intensity, compared to those under 980 nm excitation, because they belong to a higher-order photon process.[34] The second factor is that the emission intensity increases with an increase of activator concentration.[35] In our case, the content of Er^{3+} (1%) is twice than that of Tm^{3+} (0.5%) in $NaYF_4$. used in our earlier work using 980 nm illumination. Therefore, the higher rates due to the higher concentration of Er is offset by the lower rates due to the longer 1560 nm laser irradiation.

3.6 Mechanism

Fig. 7 describes the overall photocatalysis processes of $NaYF_4$: Yb,Er/CdSe composite catalysts under 1560 nm excitation, including the formation of excited levels of Er^{3+}, the activation of semiconductors via energy transfer, the charge migration between semiconductors, and the generation of free radicals. There are three steps. First, Er^{3+} has a large absorption around 1560 nm excitation,

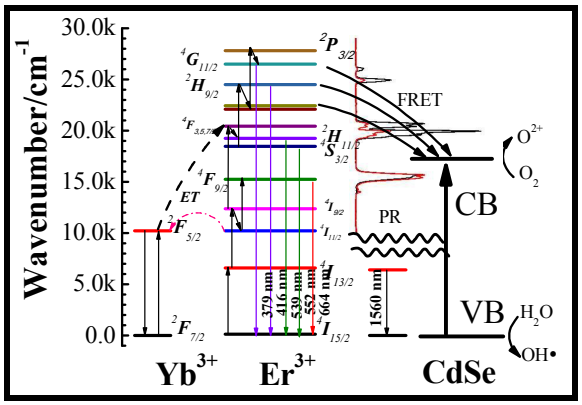

Fig. 7: Energy transfer upconversion scheme of NIR 1560 nm radiation to populate $^2H_{9/2}$, $^2H_{15/2}$, $^4S_{3/2}$ and $^4F_{9/2}$ levels of Er^{3+} ions in $NaYF_4$:Yb,Er microcrystals. The emitting levels are populated, either by nonradiative de-excitation (gray wave arrows) or cross-relaxations. The UCNPs energy is transferred to CdSe, either through FRET or photon reabsorption (PR). The corresponding conduction (CB) and valence bands (VB) of CdSe are presented.

which matches well with their $^4I_{15/2} \rightarrow {}^4I_{13/2}$ transition. Upon 1560 nm excitation, higher energy levels of Er^{3+} ions ($^2H_{9/2}$, $^2H_{11/2}$, $^4S_{3/2}$ and $^4F_{9/2}$) are populated, including ground-state absorption (GSA), excited-state absorption (ESA), and energy transfer (ET).[34] Second, the energy of these excited levels exceeds the energy gap of CdSe. According to the SEM and TEM images, $NaYF_4$: Yb,Er and CdSe are in intimate contact. This short-range interaction allows FRET to occur from $NaYF_4$: Yb,Er to CdSe.[26] In addition to FRET, there can also be photon reabsorption (PR). Lastly, the activated CdSe produces electrons and holes in the conduction band (CB) and the valence band (VB), respectively. These electron-hole pairs migrate from the inner region to the surfaces to take part in surface reactions. As shown in Fig. 7, the excited electrons arriving on the surfaces react with the oxygen adsorbed on the surfaces of CdSe to form O^{2-} or O_2^{2-}, which combines with H^+ to form hydrogen peroxide (H_2O_2).[36] H_2O_2 can react with the superoxide radical anion ($O_2^{\cdot-}$), reducing it to hydroxyl radicals ($\cdot OH$),[36] whereas, the photogenerated holes can react with H_2O to form hydroxyl radicals ($\cdot OH$).[36, 37] The $\cdot OH$ species is a strong oxidant for the partial or complete mineralization of organic chemicals.

4. Conclusions

In summary, $NaYF_4$: Yb,Er/CdSe, near-infrared photocatalysts, were prepared by subsequent deposition of CdSe nanocrystals on the surface of $NaYF_4$:Yb,Er upconversion microcrystals. XRD, SEM and TEM analysis show that the CdSe nanocrystals are in contact with the surface of upconversion microcrystals to form a heterojunction structure. UCPL spectra and time resolved spectra were used to characterize the energy transfer between $NaYF_4$: Yb,Er and CdSe. The intensity decay values of I_{decay} of 408 nm ($^2H_{9/2}\rightarrow{}^4I_{15/2}$), 520 nm ($^2H_{15/2}\rightarrow{}^4I_{15/2}$) and 539 nm ($^4S_{3/2}\rightarrow{}^4I_{15/2}$) of Er^{3+} are calculated to be 0.75, 0.80 and 0.45, respectively. However, the calculated energy transfer efficiencies for the $^2H_{9/2}$, $^2H_{15/2}$, and $^4S_{3/2}$ levels were 0.36, 0.35, and 0.20, respectively. These values show that the energy transfer processes include FRET and PR between $NaYF_4$: Yb,Er and CdSe. The decomposition of MB was carried out by the photocatalytic composites under 1560 nm laser irradiation. It was found that the rate constant was calculated to be 3.5×10^{-4} (min^{-1}) for $NaYF_4$: Yb,Er/CdSe. This rate constant is similar in value to the rate constants of $NaYF_4$: Yb,Tm/CdS under 980 nm laser irradiations,[9] The Tm concentration was twice that of Er which suggest that an increase in the content of Er^{3+} should increase catalytic efficiency under the 1560 nm laser irradiation. This study demonstrates the potential improvements in the utility rate of solar energy for photochemical and photoelectrical applications based on upconversion materials.

Acknowledgements

The authors gratefully acknowledge financial support from China Scholarship Council, This work has been financially supported by the National Natural Science Foundation of China (NSFC 11274139, 61275189, 51302103, 11474132, 11404136).

Notes and References

1. D.-X. Xu, Z.-W. Lian, M.-L. Fu, B. Yuan, J.-W. Shi and H.-J. Cui, *Applied Catalysis B-Environmental*, 2013, **142**, 377-386.
2. F. Fresno, R. Portela, S. Suarez and J. M. Coronado, *Journal of Materials Chemistry A*, 2014, **2**, 2863-2884.
3. W. Q. Fan, H. Y. Bai and W. D. Shi, *Crystengcomm*, 2014, **16**, 3059-3067.
4. Z. Wang, Y. Liu, B. Huang, Y. Dai, Z. Lou, G. Wang, X. Zhang and X. Qin, *Physical Chemistry Chemical Physics*, 2014, **16**, 2758-2774.
5. C. K. Chen, H. M. Chen, C.-J. Chen and R.-S. Liu, *Chemical Communications*, 2013, **49**, 7917-7919.
6. W. P. Qin, D. S. Zhang, D. Zhao, L. L. Wang and K. Z. Zheng, *Chemical Communications*, 2010, **46**, 2304-2306.
7. Y. N. Tang, W. H. Di, X. S. Zhai, R. Y. Yang and W. P. Qin, *Acs Catal*, 2013, **3**, 405-412.
8. X. Guo, W. Song, C. Chen, W. Di and W. Qin, *Physical Chemistry Chemical Physics*, 2013, **15**, 14681-14688.
9. X. Guo, W. Di, C. Chen, C. Liu, X. Wang and W. Qin, *Dalton Transactions*, 2014, **43**, 1048-1054.
10. C. H. Li, F. Wang, J. A. Zhu and J. C. Yu, *Applied Catalysis B-Environmental*, 2010, **100**, 433-439.
11. J. Wang, J. Li, Y. P. Xie, L. Q. Zhang, G. X. Han, Y. Li, R. Xu and X. D. Zhang, *Inorg Mater+*, 2010, **46**, 399-404.
12. S. Obregon, S. W. Lee and G. Colon, *Dalton Transactions*, 2014, **43**, 311-316.
13. S. Huang, L. Gu, C. Miao, Z. Lou, N. Zhu, H. Yuan and A. Shan, *Journal of Materials Chemistry A*, 2013, **1**, 7874-7879.
14. Y. Zhang and Z. Hong, *Nanoscale*, 2013, **5**, 8930-8933.
15. L. Zeng, L. Luo, Y. Pan, S. Luo, G. Lu and A. Wu, *Nanoscale*, 2015, **7**, 8946-8954.
16. H. Li, S. Song, W. Wang and K. Chen, *Dalton Transactions*, 2015, **44**, 16081-16090.
17. Q. Q. Dou, A. Rengaramchandran, S. T. Selvan, R. Paulmurugan and Y. Zhang, *Scientific Reports*, 2015, **5**.
18. X. Liu and J. Qiu, *Chemical Society Reviews*, 2015, **44**, 8714-8746.
19. Y. I. Park, K. T. Lee, Y. D. Suh and T. Hyeon, *Chemical Society Reviews*, 2015, **44**, 1302-1317.
20. A. Sedlmeier and H. H. Gorris, *Chemical Society Reviews*, 2015, **44**, 1526-1560.
21. N. G. Horton, K. Wang, D. Kobat, C. G. Clark, F. W. Wise, C. B. Schaffer and C. Xu, *Nat. Photonics*, 2013, **7**, 205-209.
22. J. Tragardh, G. Robb, K. K. E. Gadalla, S. Cobb, C. Travis, G. L. Oppo and G. McConnell, *Opt Lett*, 2015, **40**, 3484-3487.
23. G. F. Wang, W. P. Qin, L. L. Wang, G. D. Wei, P. F. Zhu and R. J. Kim, *Opt Express*, 2008, **16**, 11907-11914.
24. J. Aldana, Y. A. Wang and X. G. Peng, *J. Am. Chem. Soc.*, 2001, **123**, 8844-8850.
25. F. Auzel, *Chem Rev*, 2004, **104**, 139-173.
26. A. Bednarkiewicz, M. Nyk, M. Samoc and W. Strek, *J Phys Chem C*, 2010, **114**, 17535-17541.
27. C. Yan, A. Dadvand, F. Rosei and D. F. Perepichka, *J. Am. Chem. Soc.*, 2010, **132**, 8868-+.
28. Q. Zhang, P. Yang, H. S. Chen, B. B. Huang and J. X. Shen, *J Nanopart Res*, 2014, **16**.
29. Q. Shang, H. Yu, X. Kong, H. Wang, X. Wang, Y. Sun, Y. Zhang and Q. Zeng, *Journal of Luminescence*, 2008, **128**, 1211-1216.
30. H. Lu, O. Schops, U. Woggon and C. M. Niemeyer, *J. Am. Chem. Soc.*, 2008, **130**, 4815-4827.
31. W. H. Di, X. J. Wang, B. J. Chen, S. Z. Lu and X. X. Zhao, *J Phys Chem B*, 2005, **109**, 13154-13158.
32. L. X. Yu, H. W. Song, Z. X. Liu, L. M. Yang and S. Z. L. Z. H. Zheng, *J Phys Chem B*, 2005, **109**, 11450-11455.
33. G. F. Wang, W. P. Qin, J. S. Zhang, J. S. Zhang, Wangyan, C. Y. Cao, L. L. Wang, G. D. Wei, P. F. Zhu and R. J. Kim, *J Phys Chem C*, 2008, **112**, 12161-12167.
34. K. Z. Zheng, D. Zhao, D. S. Zhang, N. Liu and W. P. Qin, *Opt Lett*, 2010, **35**, 2442-2444.
35. F. Shi, J. S. Wang, D. S. Zhang, G. S. Qin and W. P. Qin, *J Mater Chem*, 2011, **21**, 13413-13421.
36. Q. Kang, Q. Z. Lu, S. H. Liu, L. X. Yang, L. F. Wen, S. L. Luo and Q. Y. Cai, *Biomaterials*, 2010, **31**, 3317-3326.
37. A. Sarkar, A. Shchukarev, A. R. Leino, K. Kordas, J. P. Mikkola, P. O. Petrov, E. S. Tuchina, A. P. Popov, M. E. Darvin, M. C. Meinke, J. Lademann and V. V. Tuchin, *Nanotechnology*, 2012, **23**.

Graphical Abstract:

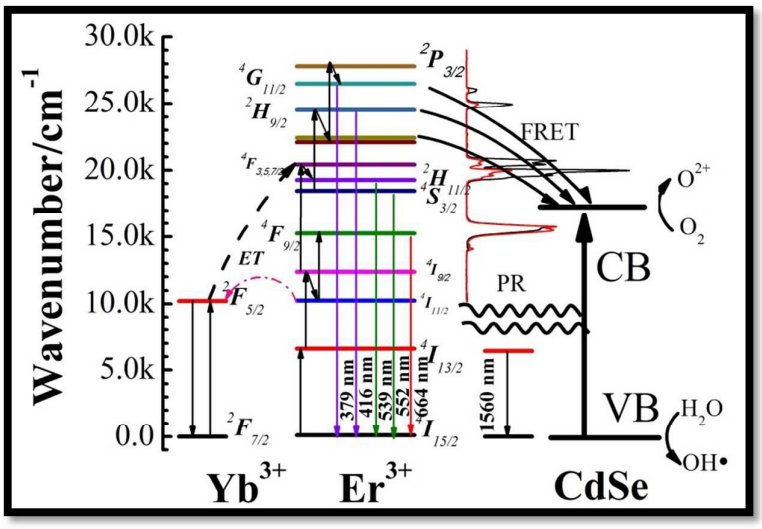

Upon 1560 nm excitation, higher energy levels of Er^{3+} ions ($^2H_{9/2}$, $^2H_{11/2}$, $^4S_{3/2}$ and $^4F_{9/2}$) are populated. FRET and photons reabsortption to occur from $NaYF_4$: Yb,Er to CdSe. Then activated CdSe produces electrons and holes in the conduction band (CB) and the valence band (VB), respectively.